ulm university universität

uulm

Institute for Electron Microscopy and Material Science

Advanced camera characterisation for low energy electrons

Bachelor Thesis
by

Luca Antonio Zangari

A thesis submitted in partial fulfilment for the degree of Bachelor of Science in University Ulm
Jenuary 2017

Examiner: Prof. Dr. Ute Kaiser

Supervisor: Dr. Felix Börrnert

1 Declaration of Authenticity

I declare that all material presented in this paper is my own work or fully and specifically acknowledged wherever adapted from other sources. I understand that if at any time it is shown that we have significantly misrepresented material presented here, any degree or credits awarded to us on the basis of that material may be revoked. I declare that all statements and information contained herein are true, correct and accurate to the best of my knowledge and belief.

Ulm, 24 Jenuary 2017

Luca Antonio Zangari

Contents

2 Abstract

In the of the Sub-Angstrom Low-Voltage Electron Microscopy (SALVE III) project to guarantee optimal imaging performances, a functioning and comparable method for a quality assessment of electron detectors is necessary. The FEI™CETA 16M camera used as one of the electron detectors in the SALVE microscope is, therefore, to be characterised by its imaging quality. In order to evaluate the point spread function (PSF) and its related modular transfer function (MFT), this thesis proposes an alternative to the established "knife-edge-method": sub-pixel illumination. With this method, a two-dimensional output is intended, together with the elimination of diffraction effects that appear with the traditional approach. For an easier and faster data acquisition, this thesis also provides a script for automatic beam tilting and image saving for DigitalMicrograph, together with a Python program for immediate data analysis and results. Datasets for the CETA camera will be created at different energies (20 kV, 30 kV, 40 kV, 60 kV and 80 kV), the MTF evaluated and confronted with the Gatan™UltraScan camera where the same measurement method is applied. The confront will show considerable differences in the imaging quality of the cameras: the CETA, using CMOS technology, will have a high level of background noise and, by comparison with the UtraScan's CCD technology, a worse PSF as well as MTF. Most crucially the results will expose how the FEI CETA camera does not achieve the level of low noise and high MTF specified by the manufacturer.

3   Motivation and purpose

Image recording is an integral part of electron microscopy. Images are recorded for analysis, archiving and publications. For a long time, photosensitive film was the only suitable choice for quality image recording in electron microscopy. This has changed with the development of the slow-scan CCD and CMOS cameras. The technology of CCD (developed in the early 1970s) and CMOS (developed at the beginning of the 1990s) have become the de-facto standard for optical imaging. The purpose of this thesis is the specific characterization of the CCD 'UltraScan' camera provided by Gatan™used by the Titan transmission electron microscope (TEM) at Ulm University and the CMOS 'CETA' device provided by FEI™used by the SALVE TEM microscope located at Heidelberg University (Fig. 1).

Figure 1: Internal view of the low voltage TEM. The double-convolution-error-correcting low-voltage TEM is the first of its kind, and even allows the recording of electron beam-sensitive materials [3]

3.1 Why use Transmission Electron Microscopy?

A microscope is defined as an instrument used to see structures that are too small to be discerned by the naked eye. The smallest distance between two points that we can resolve with our eyes is about $0.1mm$. This distance is the resolution or (more accurately) the resolving power of our eyes. So any instrument that can show us images revealing detail finer than 0.1 mm could be described as a microscope, and its highest useful magnification is governed by its resolution. The resolving power obtainable in a conventional optical microscope (VLM: visible-light microscope) is given by the Rayleigh criterion which states that the smallest distance that can be resolved, δ, is given approximately by

$$\delta = \frac{0.61\lambda}{n\sin\beta}. \tag{3.1}$$

In equation 1.1, λ is the wavelength of the radiation, n the refractive index of the viewing medium, and β the semi-angle of collection of the magnifying lens. For green light in the middle of the visible spectrum, λ is about 550 nm, and so the resolution of a good VLM is about 300 nm. Many of the features that control the properties of materials are well below the 300 nm resolution so there's a real need in nano/materials science and engineering to image details, all the way down to the atomic level. In 1924 Louis de Broglie showed that wavelength of electrons is related to their energy, E, and, if we ignore relativistic effects, we can show approximately that

$$\lambda = \frac{1.22}{E^{1/2}} \tag{3.2}$$

Here E is in electron Volts (eV) and λ in nm. In TEMs we can approximate the best resolution using (1.2) that for 100 keV the theoretical resolution would be 0.004 nm which is much smaller than the diameter of an atom [11]. Transmission electron microscopy, is then, a way to achieve

resolution up to the Å-range. Especially in applications which are aimed at the investigation of atomic structures, e.g., in Physics, Biology or chemistry, this type of microscopy is the medium of choice.

4 How to detect electrons

Transmission electron microscopy involves a high voltage electron beam that is transmitted through an ultra-thin specimen (and so transparent for electrons). The resulting spatial variation of the beam (the "image") is then magnified by a series of magnetic lenses until it is projected on a fluorescent screen, photographic plate, or light sensitive sensors such as a CCD (charge-coupled device) or CMOS (Complementary metal-oxide-semiconductor) camera. The image detected by the chip may be displayed in real time on a monitor or computer. Recent years have seen the widespread use of the charge coupled device and CMOS in all fields of TEM.

4.1 Charge-Coupled Device (CCD) detectors

CCDs are metal-insulator-silicon devices that store charge and consists of arrays up several millions of pixels. Each pixel in the CCD is an individual capacitor electrically isolated from other pixels trough the creation of potential wells under each CCD cell, in order to accumulate charge in proportion to the incident radiation intensity [11]. At the completion of a frame, to read out the pixel array, control signals, transfer the signal charge in each pixel one by one to its neighbour in the same column. At the end of each column, an output register holds the signal charge from the current pixel from that column. The charges in the output registers are then transferred one by one to the output amplifier (there can be more than one amplifier to speed up the readout). This process is repeated until all the pixels in the sensor array are read out [6].

Due to radiation damage, the CCD sensor cannot be used in the direct beam path in electron microscopes [8]. A luminescent scintillation screen is thus needed to convert the electron image to a photonic image, which is then relayed to the CCD cameras for image acquisition. The thickness and material of the scintillation layer determine how many photons will be created for each incident primary electron. Thicker scintillation layers will produce more photon signals, but will also introduce more lateral scattering by the incident electron as well as the secondary electrons and light scattering in the scintillation layer, which make the resolution worse [11]. CCD detectors have several advantages

- When cooled, they have very low noise even at low input signal levels.

- They have a high dynamic range.

- They respond linearly to changes in input signal and show a uniform response across the pixels.

4.2 CMOS Camera

Early on, conventional CMOS chips were used for imaging purposes, but the image quality was poor due to their inferior light sensitivity. Modern CMOS sensors use a more specialised technology, and the quality and light sensitivity of the sensors have rapidly increased in recent years. A CMOS imaging chip is a type of image sensor that has an amplifier for each pixel instead of the few amplifiers of a CCD; this results in less area for the capture of electrons than a CCD and with a higher electronics noise since the read-out is done pixel by pixel [9]. CMOS chips advantages include:

- Faster readout: High frames per second (fps) since read-out can be done without microscope shuttering, always collecting signal.

- Blooming: Unlike CCDs, CMOS sensors do not show any blooming

effects or smearing artefacts owing to intense illumination or overexposure.
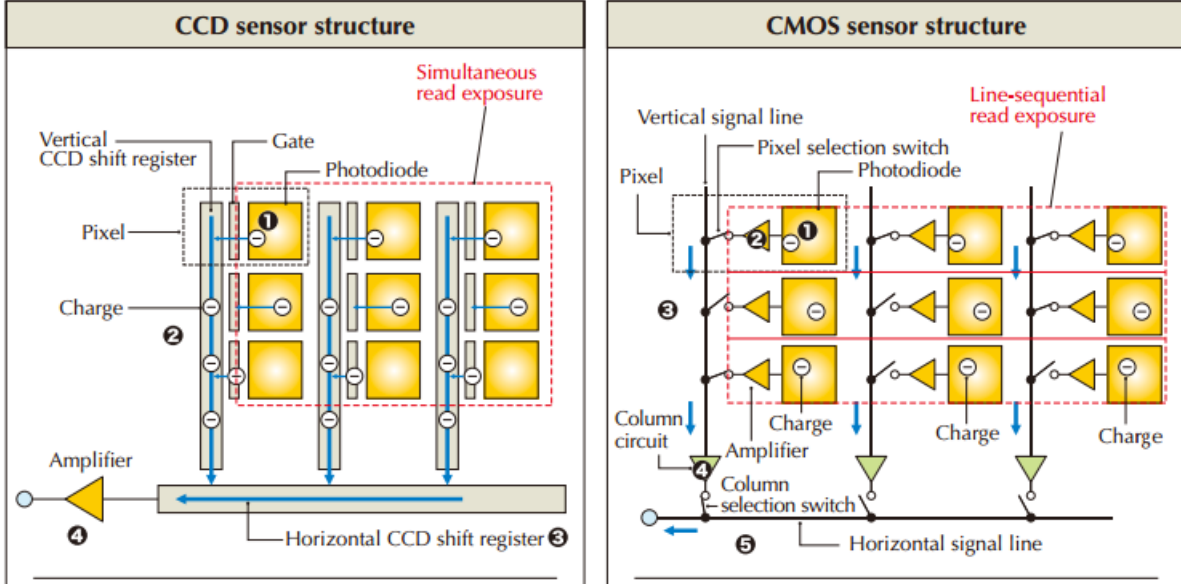

Figure 2: Electronic and structural differences between CCD and CMOS sensor chips. [1]

- **CCD:** first the photodiode within the pixel receives light which is then converted to electrical charges and accumulated in all the receiving sections are simultaneously transferred to the vertical CCD shift registers. Then the charges are transferred to the horizontal CCD shift and at last they are converted to a voltage and amplified in the amplifier, then sent to camera signal processing registers.

- **CMOS:** again the diode within the pixel receives light which is converted into electrons and accumulated. The accumulated charges are converted to a voltage by an amplifier within the pixel and transferred to the vertical signal line depending on the selected transistor. Various random noise and fixed pattern noise are eliminated by correlated double sampling at a column circuit. After CDS (correlated double sampling circuit), the image signal voltage is output through the horizontal signal line.

4.3 PSF and MTF

The chip imaging performance is described regarding two characterising functions: the point spread function (PSF), the modulation transfer function (MTF). The point spread function is one of the key features

of an imaging sensor in transmission electron microscopy. It describes the response of an imaging system to a point source. When light transferred from incident electrons by a thin fluorescent material is detected by the camera chip, the size of the emitted light is larger than that of the incident electron beam due to scattering of electrons by the fluorescent atoms. Therefore the illuminated cross-section results larger than the size of one pixel. The function that expresses the spread is called point spread function (PSF). It is, then, the two-dimensional image of a point-like object. If we apply a Fourier transformation to the PSF, it becomes the modular transfer function (MTF). The MTF is the PSF represented in Fourier-Space and indicates how the intensities of the images depend on their spatial frequency. An ideal MTF has the constant value 1 and thus transfers all frequencies of the object spectrum the same, with no modification in the image (a perfect imaging process). Looking in the real space the, corresponding PSF will be a δ-Distribution. The Modulation Transfer Function is a widely accepted way of describing the performance of an imaging system and is usually defined up to the Nyquist-limit. The Nyquist-Limit correspond to half the sampling intensity of the signal. Since the signal in the PSF is normalised to 1, the Nyquist-limit will be $0,5$ [10]. An example of the correlation between PSF and MTF is shown in (Fig. 3). The bigger the PSF width appears, and consequently the steeper the MTF is, the larger is the blurring and falsification of the image [11].
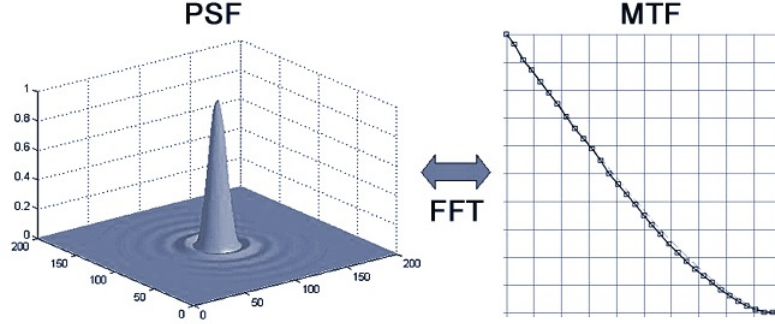
Figure 3: Correlation between MTF and PTF. In computer calculation the fast Fourier transformation (FFT) is used to compute the MTF [4].

The validity of the PSF in evaluating the performance of the camera can be understood if a specimen is imagined as a succession of infinitesimally small points (Fig.4). If a beam hits (convolute) the specimen then every point is the source of a a point-spread-function, which superpose is the final image. Thus a camera that collects the beam with a small point-spread (flat MTF) reproduces the object more faithfully since the superpositions of the PSFs are small. A camera which scintillator produces a wider PSF will reproduce the image blurred and falsified thus not being optimal for the very small structures that a TEM needs to observe.

Figure 4: Schematic representation of the PSF´s origin and how the image can be described as an overlapping of different PSFs.

10

4.4 Noise generation in CCD and CMOS cameras

All the components in an acquisition camera contribute to the noise. There are typically four physical stages in the detector (Fig. 5):

- Reflection layer: Input noise

- Scintillator: Shot noise and random scattering

- fibre optics: Random annihilation and scattering of photons

- Sensor: Statistical electron-hole pair generation and dark current as well as electronics noise

Firstly primary electrons impinge the scintillator layer. This layer, typically made of phosphor, is where various excitations processes scatter electrons, some of which produce photons after relaxation (for an overview see [6]). Additionally, these photons are scattered within the scintillator before they enter the second physical stage of the camera (fibre optics). There the photons might be further dispersed, absorbed or backscattered from the fibre optics into the scintillator (where they again produce photons) [7]. Finally, the photons are absorbed in the chip, where statical electron-hole pairs are generated. After the exposure, these accumulated charges are transmitted to the computer and digitalized as arbitrary digital units (ADU).
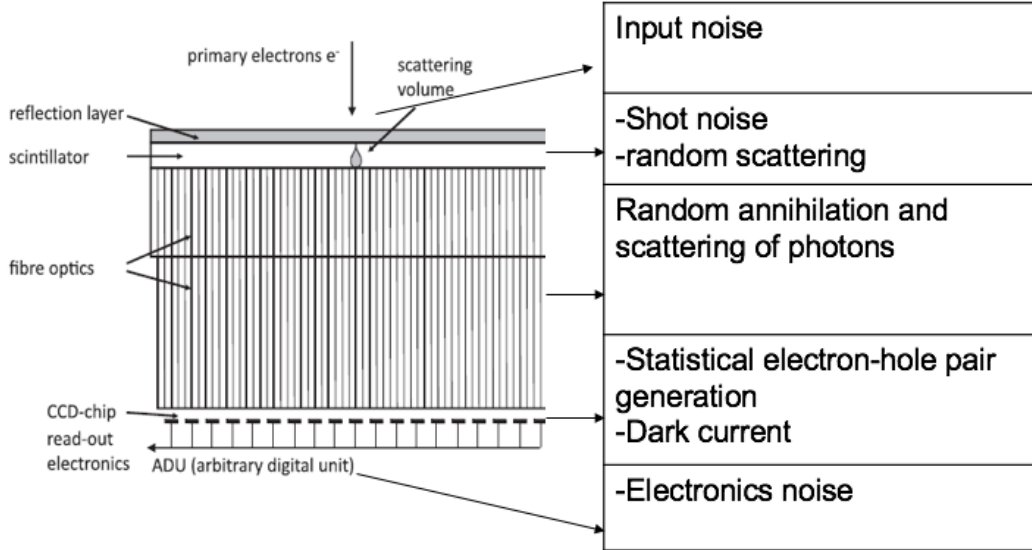
Figure 5: Noice generation [7]

All this process contribute to the formation and distortion of the final image are affected (see 4.3). In (Tab. 1) is an overview of the level at which the PSF and Conversion Rate (CR) (see sec. 4.5) are affected. In the first layer scattering and reflection take place which creates a bulb of photons that define the PSF. The bigger this bulb, the wider will the point-spread be. Again in the fibre optics scattering contributes negatively to the final PSF as does the diffusion in the readout chip. Also, the conversion rate is affected at the different levels: as the interaction cross-section of the scintillator thickens the CR rises. In the fibre optics photons are lost due to absorption and again altered in the readout process.

Level	Point spread	Conversion rate
Reflection layer and scintillator	Scattering and Reflection	Interaction cross section
Fibre optics	Scattering	Absorption
Chip and readout	Diffusion	Interaction cross section

Table 1: Error type contribution

To make a valid statement about the quality of different cameras, it is necessary to quantify the conversion rate as well as the PSF (and consequently the MTF).

4.5 Conversion rate

The conversion rate of an electron detection camera is the ratio between the digital units ("counts") contained in the image and the number of electrons ("e^-") recorded by the chip. Since quantities in the acquired image can only be measured in units of counts, knowing the conversion rate is highly important. This value is relevant for the manufacture because adjusting it permits to overcome the background noise: high level of noise are surmounted with more signal, and therefore a higher conversion rate are required. In TEM usage this value is relevant in order to know the exact number of charges that pass through the specimen. As mentioned in (4.4) incoming electron are scattered in the scintillator where they excite its atoms. The result of this excitation are photons which pass trough the camera optics and are back-transformed to electrons. Therefore the conversion rate strongly depends on the thickness and material of the scintillator. A thin scintillator has a small interaction volume where the scattered electrons excite the atoms. This means that fewer photons are generated, fewer electrons detected and therefore the conversion rate is small. A thick scintillator has a bigger interaction volume, and consequently, more electron-atom interaction, also due to diffraction since the travelling distance of electrons is longer. After being back-transformed, cameras with a thick scintillator will detect more

13

electrons and have a higher conversion rate. The choice of the right scintillator that results in the correct conversion rate is a delicate balance between overcoming the background noise and have enough electrons left to have a good signal, firstly because the charge reaching the chip must be sufficient to provide a signal well above the noise level. The thickness of the scintillator membrane, therefore, impacts the PSF directly and is dealt with great secrecy by the manufacturer. Nonetheless we can assume that cameras with a thin scintillator and with low conversion rate, improve the PSF because of its narrow interaction volume, the signal output is stronger and the PSF consequently higher. The point-spread is influenced negatively by a scintillator which is too thick: the interaction volume is large, and the so is the scattering blob.

5 Measurement method and evaluation

5.1 Measurement of the conversion rate

The conversion rate (CR) is defined as the ration between the mean value of all counts and an electron:

$$CR = \frac{\langle counts \rangle}{e^-} = \frac{\sum (counts)}{\sum e^-}. \tag{5.1}$$

Here $\sum counts$ is the sum over all digital counts in all pixel of the chip and $\sum e-$ the total number of all hitting the chip. It is given by

$$\sum e^- = \frac{Q}{e} \tag{5.2}$$

where Q is the total charge on the chip and e the elementary charge. The total charge Q can be derived from

$$I = \frac{Q}{t} \tag{5.3}$$

where I is the electric current hitting the camera and t the time of exposure. The conversion rate can now be evaluated as:

$$CR = \frac{\sum (counts)}{e} \cdot It \tag{5.4}$$

The detected current is the beam-current I_b collected on the fluorescent screen located before the camera. To make sure that I hitting the camera and I_b are the same, the set-up in (Fig. 12) is prepared. A circular mask is applied in the path of the electron beam. The size of the mask determines how much electron beam passes trough. The bigger the hole in the mask the bigger the total current measured and the better the statistics. The mask cannot be larger than the chip itself because it is crucial to count all incoming electron. If the hole were to be greater than the chip, numerous charges would simply fly by without being detected. The detected I_b is

15

now the same as the I hitting the camera. The exposure time t is set constant and the $\sum(counts)$ is calculated by the readout program which sums up all pixels values. The conversion rate can now be determined and plotted. Results for the FEI Ceta and UltraScan Camera for different energies are reported in (Fig. 13). For comparable values of energy at 80 kV, there is a factor 4 difference between the UltraScan and the Ceta camera. We can claim that this difference can be traced back to the scintillator; more precisely the scintillator is thinner in the UltraScan than the CETA camera. Since in the UltraScan the conversion rate is 4,2, for every primary electron approximately five counts are assigned. This low value indicates that many electrons are detected and therefore pass trough a thin scintillator. Being a CCD-type of detector the noise is low and can be overcome with very few counts. This leaves room for more clear signal until pixel saturation. It can also be assumed that the FEI Ceta camera will have a higher background noise since it is a CMOS type of detector and the higher CR at 80 kV confirms it. Comparing this with the UltraScan camera results in a four times weaker signal in same conditions. Pixel saturation is also reached more quickly. From (Fig. 12) can be read that for lower energies the conversion rate of the Ceta camera decreases approximately linearly from 15,1 $counts/e^-$ at 80 kV to 32,8 $counts/e^-$ per primary electron at 20 kV. The velocity of the electrons is proportional to their energy, so lower energy charges will have a longer permanence in the scintillator increasing the interaction volume and also the value of the CR. Assumption over the PSF can also be made. The UltraScan's low conversion rate will results in a sharper PSF due to its smaller scintillator and smaller interaction volume. The FEI Ceta camera will have a wider PSF since the primary electrons scatter in a bigger interaction volume. The PSF for both cameras and different energy are evaluated in chapter (5.5).

Figure 6: figure
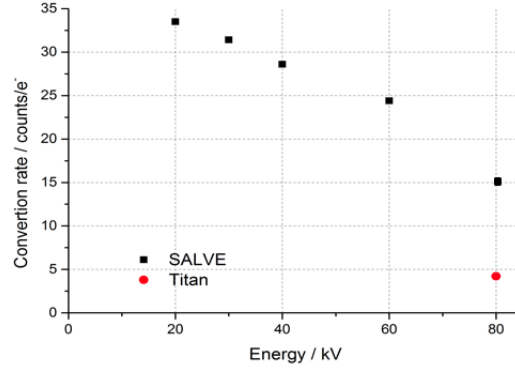Conversion rate camera set-up.

Figure 7: figure
Conversion rate for different energies and cameras.

5.2 Noise only

To determine if the conversion rate is calibrated correctly and can overcome the background noise level, simple raw images with no illumination are taken and evaluated. An example of this image can be seen in (Fig. 8). Since no pixel is illuminated by the electrons from the microscope, its value is determined only by the background noise level. Expected is that CMOS cameras (FEI CETA) have a higher level of background noise than CCD (Gatan UltraScan) chips since they have fewer electronics as part of their construction.
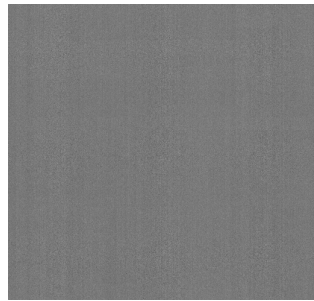
Figure 8: Example of a non illuminated image where the pixel values are generated from noise only.

FEI equipped their camera with a 'noise reduced' mode that promises to diminish the background interference; the extent and functionality of this mode are not provided by the producer. In (Fig. 9) the normalised amount of pixel per count value for the two different devices is plotted and compared.
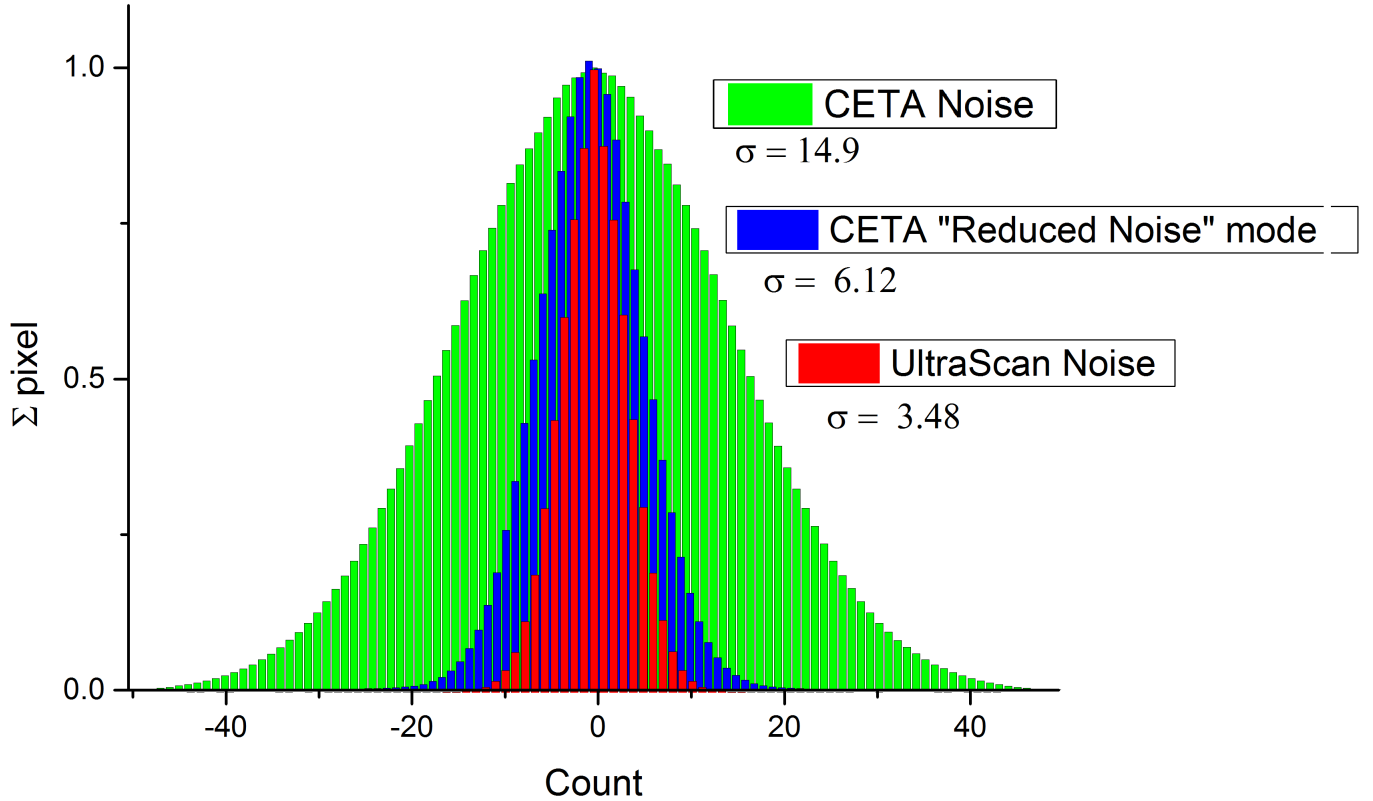
Figure 9: Noise only comparison between UltraScan (red), CETA normal mode (green) and 'noise reduced' mode (blue).

The standard deviation gives the average amount of counts that characterise the background noise are spread over the pixels of the camera. The conversion rate needs to be enough to counterbalance the noise. The

σ values for the normal CETA readout and the UltraScan are consistent with the evaluated conversion rates in section (4.5) (Fig. 7). At an average noise level of 15 counts/px in the CETA, corresponds a CR of 15 counts/e. This means that for the signal's information, that about electron is needed to overcome the noise and is buried under it. Same for the UltraScan where the σ=3.48 and the conversion rate is 4,2. For the 'reduced noise' mode, only the information carried by every 3rd electron is lost. Adjusted for the conversion rate (at 80 kV for comparable results), the *sigma* gives now exactly the number of electrons that are needed to overcome the noise (Fig. 10).
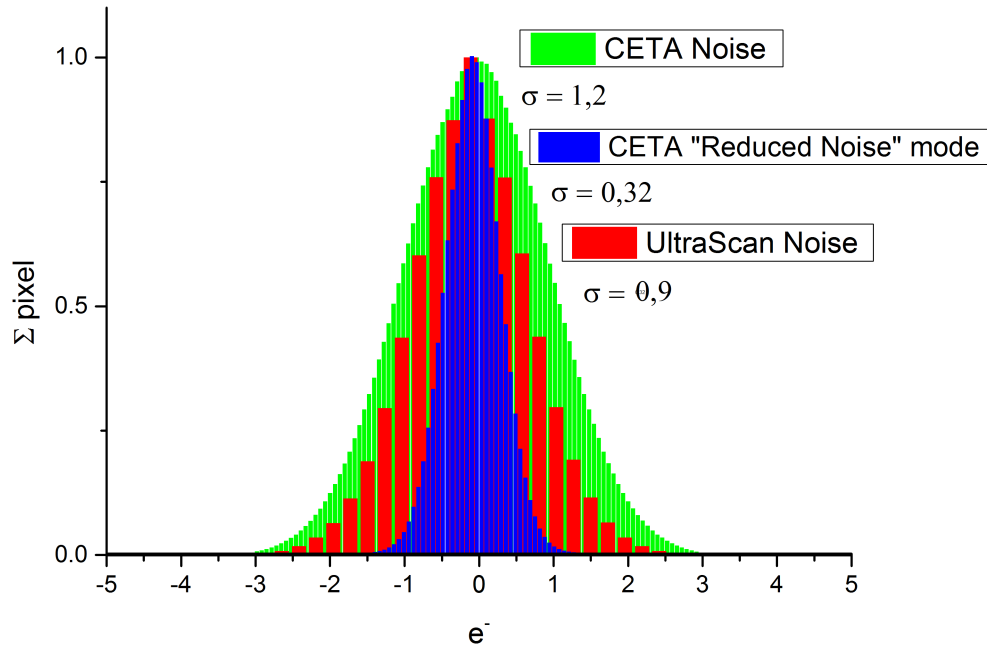
Figure 10: Noise only comparison adjusted for the CR between UltraScan (red), CETA normal mode (green) and 'reduced noise' mode (blue).

These results indicate that the conversion rate was calibrated correctly

at 80 kV. For different energies such as 20 kV where the CR is double the one at 80 kV, the 'noise reduced' mode, maybe useful to counterbalance the fewer number of electrons hitting the readout chip.

5.3 Measurement method

The standard method with which the PSF is determined is the so-called "knife-edge" method (Fig.11).The edge method measures the response of an imaging system to an input of sharp edge transition created with a blocker put in the path of the electron beam. The two main problem of this method are: one dimensional outcome (from the knife edge away) and the diffraction phenomena since the knife is at a given distance from the camera and the electrons experience diffraction.
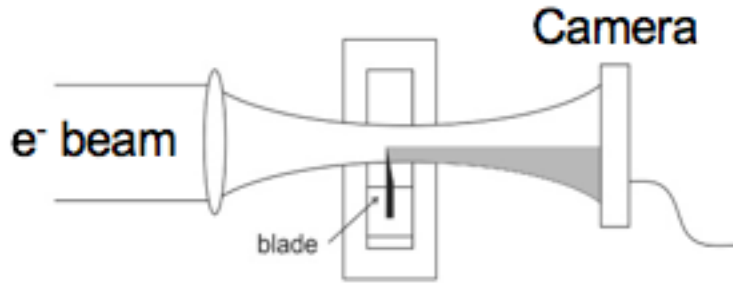
Figure 11: Schematics of the knife edge method [5].

To get around this limitations, the method of a subpixel illumination is proposed. The electron beam is to be focused so that its cross-section is significantly smaller than the size of one pixel (Fig. 12). With this method, the output will be two-dimensional (x and y-axis of the chip), and there will be a direct illumination on the camera with no further form of diffraction between the electron beam and the scintillator.
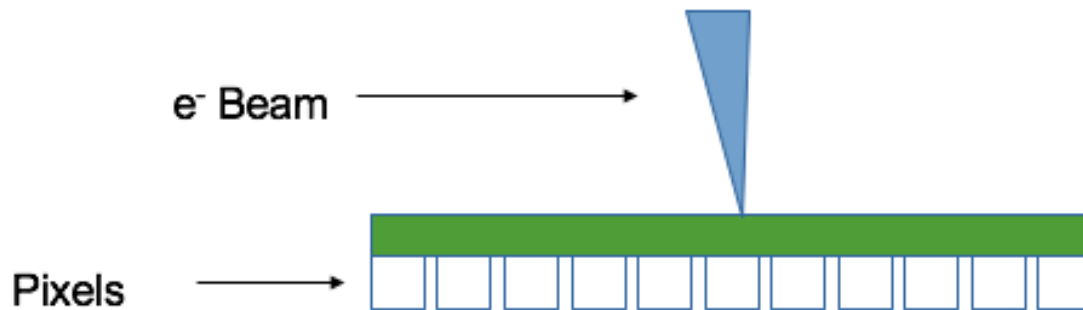
Figure 12: Schematics of the subpixel illumination method: a highly focused beam hits the scintillator directly and illuminates the chip. Its cross-section has to be significantly smaller then the with of a pixel.

The highly focused beam after hitting the scintillator and passing through the optics of the camera will reach the chip's electronics where it will be registered as a pixel value. The focused beam can now land either inside or on the edge of the pixel. Looking at the intensity distribution, we can distinguish the two cases (Fig.13):
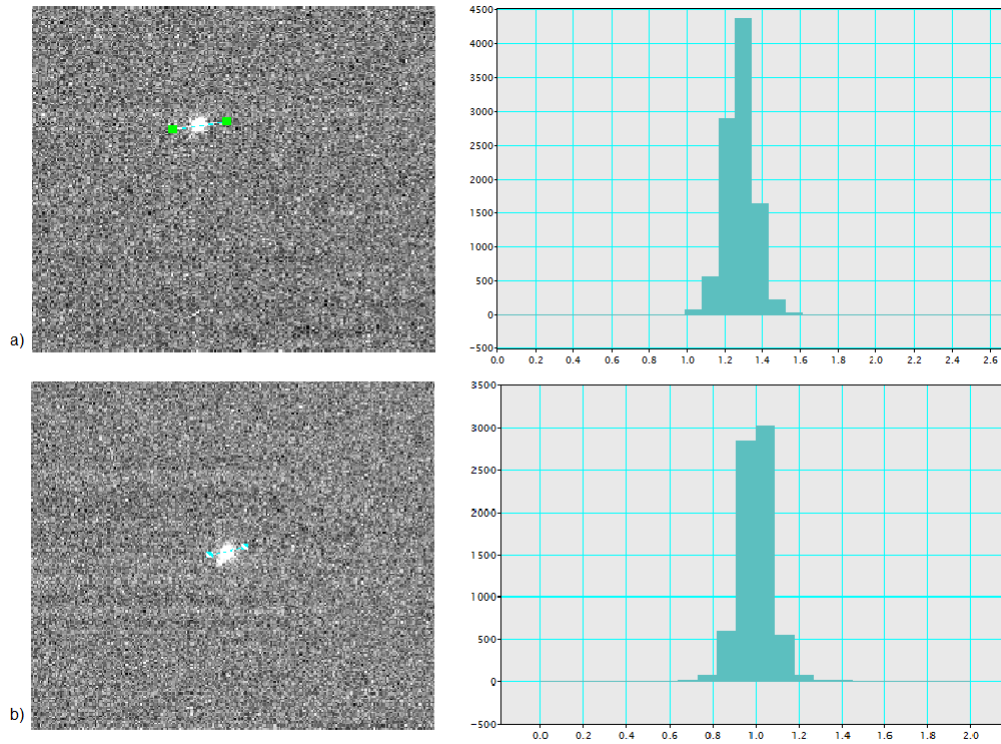
Figure 13: Possible scenarios for incident electron:

- a) The beam landed inside a pixel: the intensity distribution has a clear peak on the illuminated pixel.

- b) The beam landed on the pixel's edge: the integration over the distribution remains the same but the maximum intensity will be lower and shared with the neighbourly pixel.

After the beam is prepared to be smaller than one pixel (**??**) the dataset can be acquired. To overcome the pixel-oversampling, it is necessary to record many images. The standard oversampling rate 4x means that the pixels are divided in 16 sub-pixel and that by taking 1000 images the dataset will consist of $1000/16 \approx 62$ images per sub-pixel region. Since we cannot know exactly where the beam is hitting the pixel, for every image it has to be shifted randomly along the chips area. The more

images are taken, the more statistically relevant the dataset becomes. This erratic shifting can be done manually or by using the DigitalMicrograph™script provided with this thesis (Sec. 6.1). The dataset will then consist of numerous images with a bright maximum at different points on the chip area on oversampled pixels. This random positions can be projected on a single virtual pixel, so it is covered evenly by the illuminated points (Fig. 14).
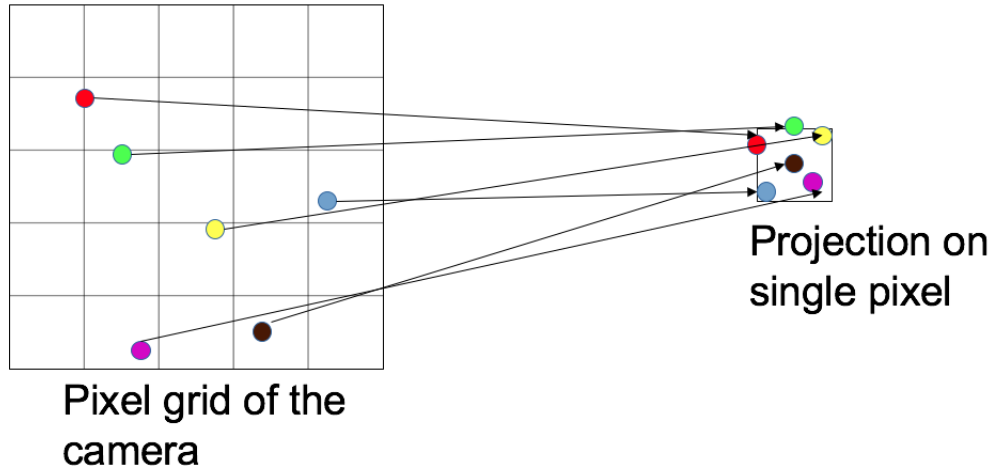

Figure 14: Schematics of the "cramping" process.

5.4 Test for sub-pixel region

To check if the beam is really in the sub-pixel region the following method is proposed. After focusing the electron flow to a narrow beam, the camera length is progressively decreased. In microscopy, the camera length (CL) is the distance from the sample to the projected image. The diffraction pattern forms the projected image on the screen and can be recorded, hence the term 'camera length' since this is where the camera is positioned [11]. In our specific case, there is no specimen where the beam is scattered, so the CL is simply the virtual distance from the sample

holder to the acquisition device; virtual because the camera length is a calculated value rather than a physical distance. It can be changed by increasing or decreasing the magnification of the lenses between the sample holder and the viewing screen. For the measurement, the initial CL is set on 2,7 m and is decreased progressively to 3 mm in 20 steps. In the beginning, the beam is focused so that the integrated intensity is in a safe zone (under 10000 counts) to not compromise the integrity of the camera. The camera length is then decreased by one step: this reduces the beam's full width at half maximum (FWHM), increases the maximum intensity and leaves the integrated intensity unaltered (Fig. 15).
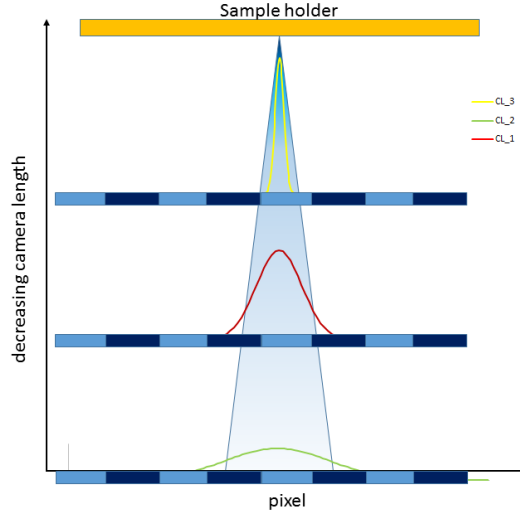
Figure 15: Theoretical representation of incident electron beam at different camera length (CL_1>CL_2>CL_3). For smaller camera length the beam sharpens, decreases the FWHM and increases the maximum intensity until the 1 pixel limit is reached (CL_3 smaller than one pixel). Real, measurable distribution are of course not continuous but discreet.

At every step the CL is notated, an image is taken and the beam adjusted to prevent astigmatism. Theoretical exceptions are therefore that

by decreasing the CL no change in integrated intensity happens, that the maximum intensity should progress quadratically and that the FWHM of the beam will decrease linearly. Both the FWHM and the maximum intensity will reach a constant level when the single pixel illumination limit is hit (Fig. 16).
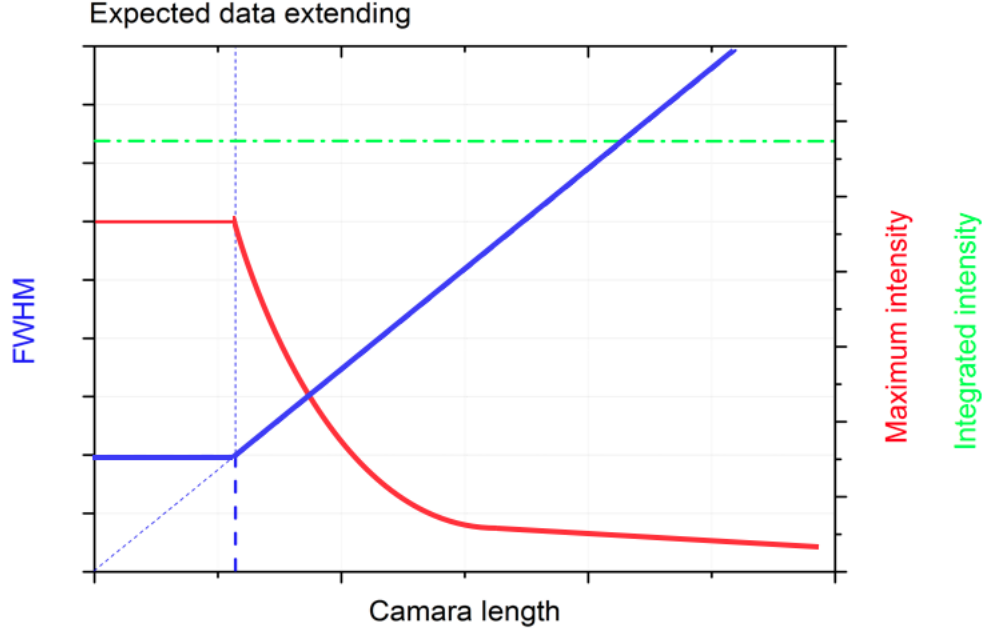
Figure 16: Expected data extending for changing camera length. The sub-pixel region begins at the FWHM minimum.

When this limit is hit the pixel is now bigger than the FWHM so no further changes can be displayed: the definite information limit is reached. This does not mean, however, that the beam cross-section does not continue to get smaller along with smaller the camera length. We can interpolate the real size of the effective beam cross- section from the data plotted in (Fig.17) and (Fig.18). At around 30 cm the theoretically perfect illumination should be exactly one pixel in size. Since the following measurements do not change and the last measurement remains the

same at a distance of 30 mm we can assume that the beam is prepared at 1/10 the size of a pixel.
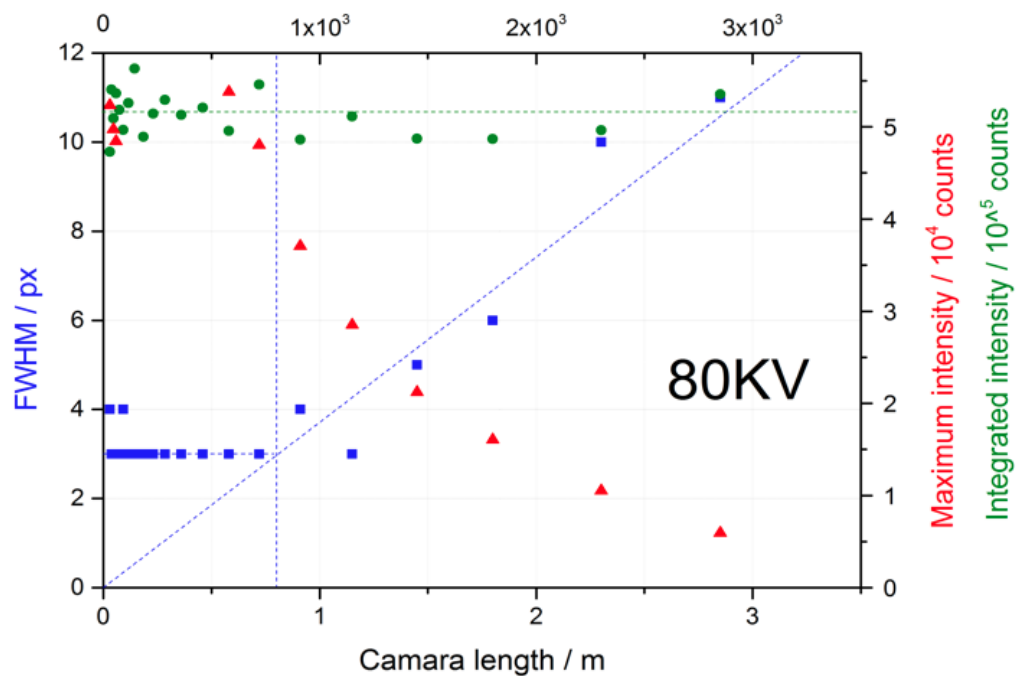

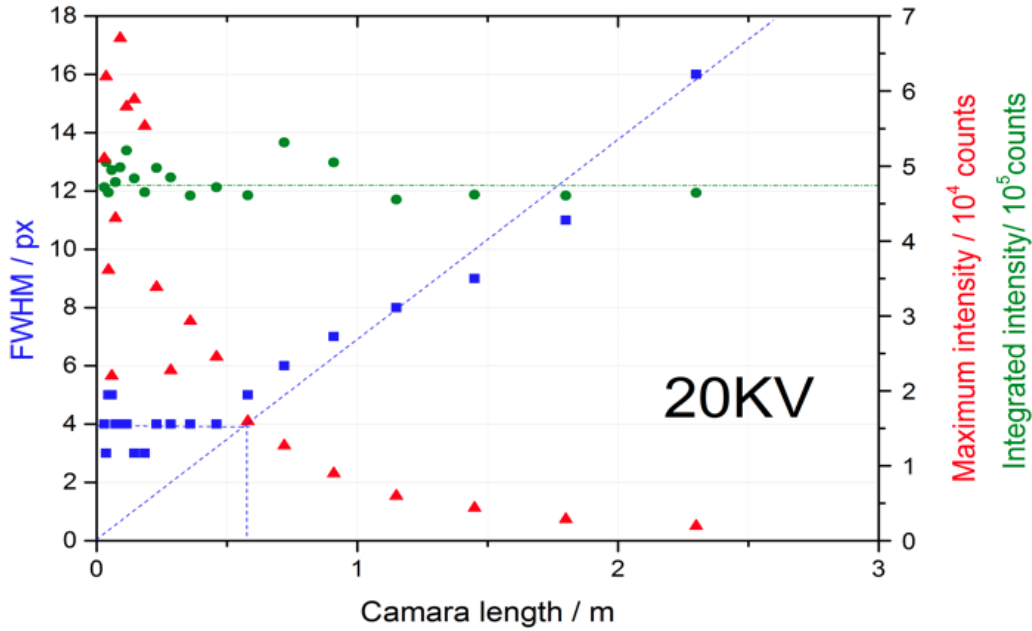Figure 17: Illumination size at 80 kV for the SALVE microscope.

Figure 18: Illumination size at 20 kV for the SALVE microscope.

The data for 80 kV and 20 kV for the CETA camera is mostly consistent with our expectation 16. At 80 kV the total illumination behaves almost constantly. FWHM decreases and remains constant (within a read-out error of 1 pixel) at its supposed rate and the maximum intensity grows approximately quadratically. At 20 kV behaves similarly with occasional inconsistent values in the maximum intensity.

5.5 Point illumination data creation and analysis

After the TEM is set at the chosen energy and beam is prepared with the method presented in section 5.4 the measurement is started: 1000 were taken for every energy on the CETA device (20 kV, 30 kV, 40 kV, 60 kV and 80 kV) and 80 kV on the UltraScan device. This data is then analysed with the python program presented in section 6.2 where the

statistical PSF and MTF over all images is calculated. The results are stored and plotted in (Fig. 19) and (Fig. 20). The intensity is normalised between 0 and 1.
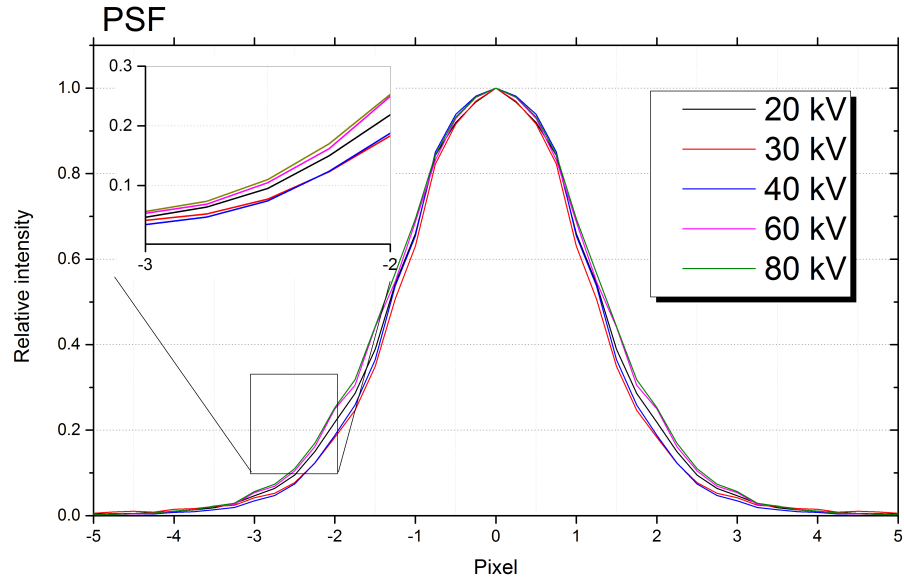

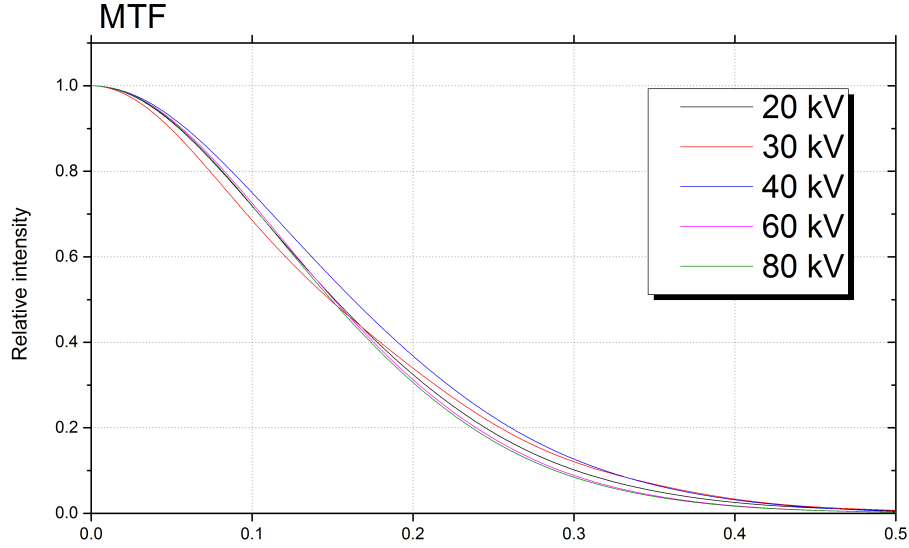Figure 19: PSF for the FEI CETA camera for different energies with normalized intensity.

Figure 20: MTF for the FETI CETA camera at different energies.

As explained in section 4.5 the PSF will results wider for lower energies since the electrons have a larger interaction volume generating a bigger scattering blob. The results show that the 80 kV PSF (highest energy) is the widest which is inconsistent with the prediction. This can also be seen in the MTF where 80 kV is the first to approach 0. The fact that the PSFs for different energy are not in order from the weakest to the strongest suggests that the scintillator behaves strangely at different energies. The cameras best performance is given at 40 kV: it can be clearly seen its the MTF which slope is smaller than the next best energy (30 kV). For 60 kV and 20 kV, the performance is very similar. Comparing this results with the UltraScan camera, it becomes clear that the imaging process of the CETA camera is not optimal. In (Fig. 19) and (Fig. 20) the results at 80 kV for the two camera are compared. The PSF for the UltraScan appears narrower than the CETA: if we compare the FWHM there is a

29

difference a factor 1,5 (2 px for the UltraScan and 3 px for CETA). For reference looking at the Nyquist-limit, the UltraScan hits it at $0,1$ relative intensity and the CETA is almost 0 (instead of the advertised 0.10). Since conversion rate has been calibrated correctly as shown in section (5.2), this difference can be explained firstly by the thickness of the scintillator and secondly by the higher noise level that occurs in the readout process. The scintillator being thicker in the FEI CETA camera, offers a bigger interaction cross-section for electrons: the resulting bulb is, therefore, larger and so is the consequently detected PSF. The higher noise level also contributes negatively to the final performance of the camera: as seen in (Fig. 9) the background noise is five times larger than the average interference in the CCD chip. The compensation with a higher conversion rate is not enough to guarantee the promised performance of 10% at Nyquist-limit for which this camera was chosen as main acquisition device for the SALVE project.
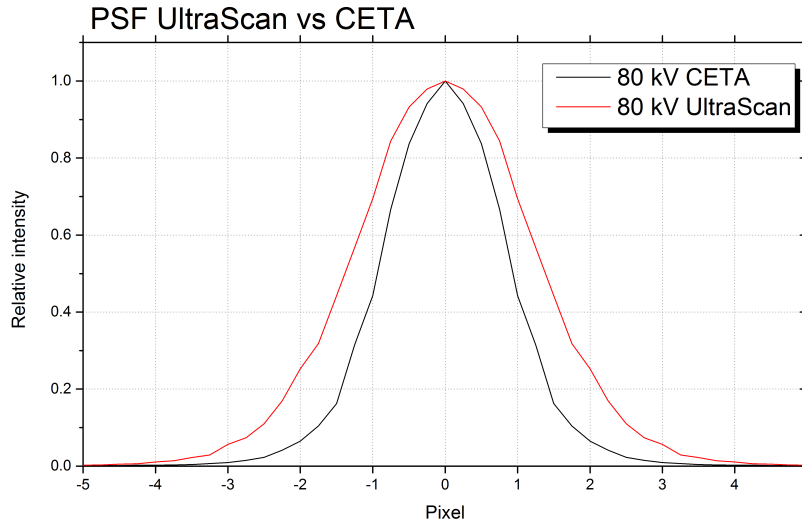

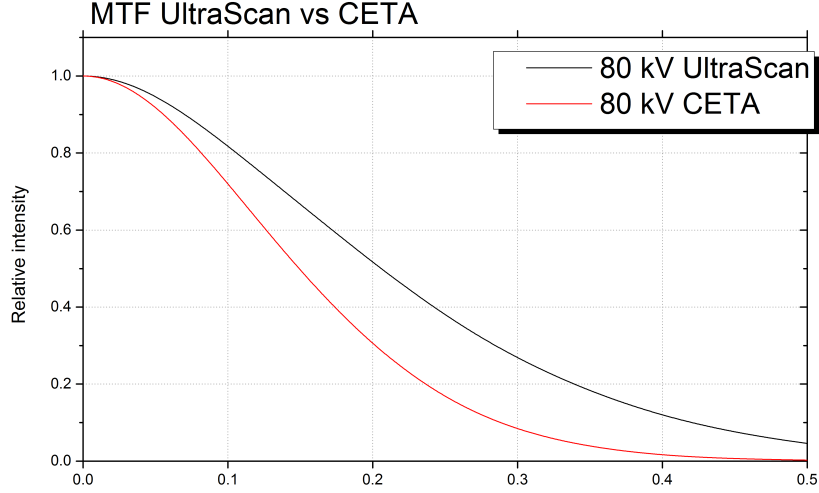Figure 21: PSF comparison between SALVE and Titan microscopes.

Figure 22: MTF comparison between SALVE and Titan microscopes.

In (Fig. 23) the PSF at 80 kV for the two cameras are plotted in a weighted 2D image. In the UltraScan single pixel are illuminated symmetrically with a maximum in the middle. In the CETA 2D PSF, the representation of the blob is asymmetrical and distorted. Also, the maximum is not well defined and the relevant area approximately twice as big as the UltraScan Camera. The distortion in this representation can be traced back to the shutter of the SALVE microscope that cannot be controlled manually. The shutter is a magnet that deflects the beam onto the camera when it is needed. The shutter in the SALVE microscope actives as soon as the camera starts its exposure time. This means that the movement of the beam across the chip until it reached the desired position, is also imprinted on the readout electronics altering the acquisition.
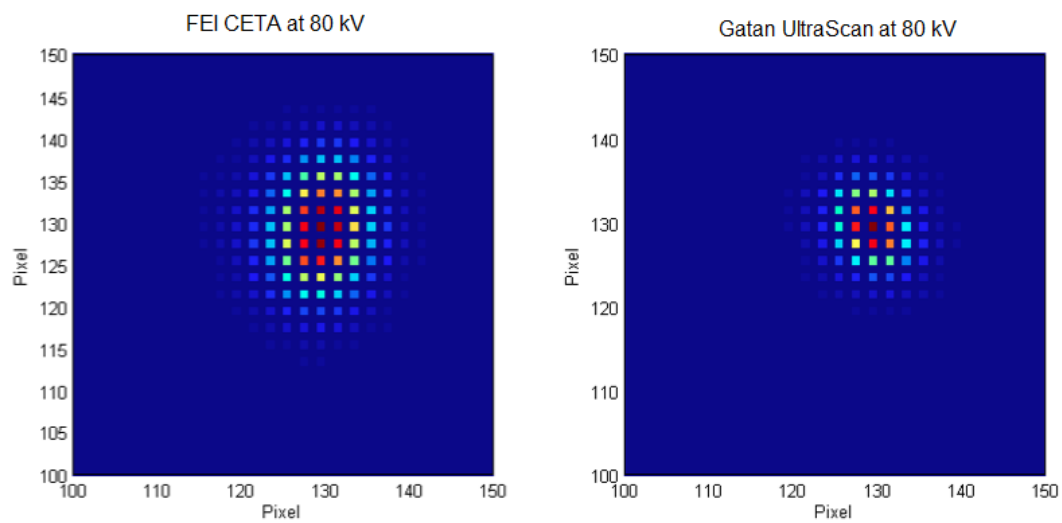
Figure 23: figure
2D plot of PSF at 80 kV for the two cameras. CETA camera presents a considerable asymmetry.

6 Provided acquisition and evaluation programs

6.1 Automatic image acquisition process

It is estimated that for a relevant statistical expression much data is needed. The procurement process is simple but very long and tedious. The measurement process involves a and random repetitive tilting of the electron beam in the diffraction mode. After every tilt, an image is taken and saved to a local hard drive. By using the script function in Digital Micrograph, an atomization script has been provided. This script will firstly display some prompt for the user:

- Label: the user is asked if he wants to label the images. The default value is 1 which means yes. 0 would mean no.

- Number of images: this prompt is used to set the number of images to collect. The default value is 100.

- Binning: this prompt permits to choose the binning value if one is desired. Possible inputs are 1,2,4 and 8.

- Exposure time: the user can choose the desired exposure time of the chip. The default is 1 second.

- Chip Dimension: the user should enter the Chip dimension. Default is 2048

  Before starting the script, the illuminated point should be in a central position. From there random numbers are generated and added to the *EMBeamTilt* function. This function tilts the beam and positions the point on a random location on the chip. Since every random shift number starts from the initial position, the point will not go out of the field of view provided the range be selected correctly. After every repositioning, an image is taken and saved at the desired location. This loop is repeated until the desired number of images is acquired.

6.2 Why Python

After the acquisition of the dataset, it is practical to have an evaluation program that can process this stack of data automatically. This can be done in a variety of programming languages. Matlab for example as a numerical computing environment that allows good Matrix manipulation could be a good candidate for the task at hand. Limitations of MatLab include a mostly inefficient use of resources and large size of the raw code. The second obvious candidate is Python. Python is a powerful, flexible, open source language that is easy to learn, easy to use and has powerful libraries for data manipulation and analysis. Its simple syntax is very accessible to programming novices and will look familiar to anyone with experience in Matlab, C/C++, Java, or Visual Basic. Python has a unique combination of being both a capable general-purpose programming language as well as being easy to use for analytical and quantitative computing. The Python programming language also is completely free to use and has an excellent compatibility with virtually any operating system. A large part of this thesis consists of writing data-preparation functions for large image stacks and of the translation of the evaluation program from MatLab to Python. With the complete routine, it is possible to give a single folder with raw images as input and have an output folder where all the results are saved for future plotting. A preview of these results is also provided. The following will describe the structure and processes made by the program.

6.3 Program structure

Needed Python modules:

- numpy, scipy, matplotlib, math
- PIL (pillow), tifffile, libtiff, pickle
- dm3lib , tia_reader, ReadDMFile [2]

The evaluation program consists of two main classes:

- stack_image_v2.py: Execute this file to start the evaluation. It will accepts 3 parameters: –srcdir [path to input folder] –output [path to output folder] –size [NxN size of the stack (default 64x64)]. This class will first scan the input folder and determine what kind of images are to be processed. It will accept .ser , .tif and .dm3 formats. For every image, it will find the maximum and cut a 64 by 64 square around it reducing the size of the data greatly. For example 1000 images a. 16 Mb per image (a total of approx. 16 Gb) are reduced to a single 16 Mb stack of images. This process of cutting down is useful since the relevant information is stored at and around the brightest point. The cropped images are now stacked so that now one single .tif file is created where the brightest pixel is always at the centre of every image in the stack. The cropped images are now processed by the main program (single_pixe_finall_all.py).

- single_pixe_finall_all.py: The first 20 lines of Python code are simple `import` directives. These are used to tell the Python interpreter which libraries to utilise. Some of these libraries are used to provide numerical computing algorithms, and others are used to provide plotting capability. After this, several auxiliary functions are defined to enable more parity with MATLAB in the main body of the code. These functions emulate the MATLAB counterparts since the base Numpy libraries either do not include these functions as standard or chose a different set of defaults. Two of these functions are simple coordinate transformation functions. The other two are convolution functions. The base Numpy convolution functions work the same as the MATLAB functions in "full"[1] mode. In this code, the "same"[2] mode is desired, but is not a provided option. As a result, the "full" convolution is performed, and the center section of the vector is re-

---

[1] Full convolution produces an output vector with length $L = M + N - 1$ for M, N length input vectors
[2] Center convolution, using only the middle $\min(M, N)$ elements

turned. The function `processdata()` is the main body of the script. Python, like MATLAB, executes the main script file from top to bottom in general. However, it does not execute the first function. It continues through the source file until it finds a main entry point, similar to the `int main()` function in `C`. In Python, the entry point is defined as:

```
if __name__ == "__main__":
    processdata()
```

This allows numerous functions to be defined in the same Python file, but control which files can be directly executed. It is a Python programming custom - though not a requirement - to place the main entry point definition at the end of the source file. The code in `processdata()` begins with several processing parameters, similar to the MATLAB version. These are included for flexibility by allowing different oversampling rates and other parameters to be changed without modifying the rest of the script. After the dimensions of the processing image have been defined, coordinates are calculated for every pixel in the image. The liberal use of `temp` variables is for debugging purposes, by allowing intermediate steps in the corresponding single line of the MATLAB script to be inspected at run-time. Once the coordinates have been defined, the image data is loaded from a defined file in one of the several formats (.ser, .tif, .dm3). Once the data is imported into a Numpy array, the data needs to reshaped for easier analysis. While MATLAB uses a vector to define the dimensions of an array, Python uses a different data structure called `tuple` for this purpose. As a result, simple element-wise multiplication cannot be directly performed, since a tuple object replicates when multiplied. This behaviour is due to operator overloading since tuple objects cannot be modified. When a tuple is multiplied by an

36

integer N, it replicates the data in the tuple N times. Another important distinction between MATLAB and Python is the way arrays are handled. MATLAB passes arrays as copies by value, whereas Python passes arrays by reference. As a result, to duplicate arrays, the function `numpy.copy()` must be used. After this, the global intensity of each image in the set is computed, and the mean and standard deviation of global intensity across the image set are calculated. To make this process easier, the image data is stored in a 3D matrix structure, with the first two dimensions being each image, and the third dimension being the number of the image in the set.
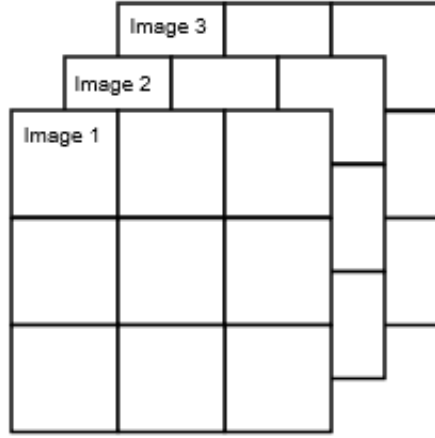
Figure 24: Shape of the images stack.

For each image, the local area is oversampled using real space oversampling. The oversampling value is a constant 4. This data is used to estimate the point spread function (PSF) and Modulation Transfer Function (MTF). Because the PSF is defined as a convolution integral in two dimensions, the two-dimensional Fourier Transform is used to compute this. Because of the computational efficiency of computing the Fast Fourier Transform (FFT) versus the discrete

convolution, it is more efficient to compute the FFT of the signal, multiply it in the frequency domain, and IFFT it back to the time/spatial domain.

$$conv(x, y) = IFFT(FFT(x) * FFT(y)) \qquad (6.1)$$

Once the image has been centred as accurately as possible given the oversampling level and convergence criteria, the image is downsampled back to its original resolution. Since each of the images has the max covariance centred, the images are averaged together to produce an average image covariance. The average image is used to compute the PSF as a function of radius with a p-chip interpolation function. Since the pixel radius from the center of the image was computed early on, the individual radii to each pixel can be calculated in increasing order. For each pixel in the given search radius `rmax`, the number of non-zero covariance values is calculated. This figure is used to generate the PSF value for a given radius from the center of the image. The PSF as a function of radius is then oversampled using the FFT technique again. From this, the MTF is calculated. Because of the padded PSF data, the MTF array is truncated back to the size of the original PSF matrix. Once the MTF is calculated, it is plotted with the PSF.

6.4   Python Auxiliary Functions

While Python+Numpy has many comparable functions to MATLAB, there are several key differences in the documentation. Several auxiliary python functions were therefore written to enable the body of the script to appear much more similar to the MATLAB version of the script. A list of these auxiliary functions is included below:

- `conv2`: 2-dimension convolution

- `conv4`: 4-dimension convolution
- `cart2pol`: Cartesian to Polar coordinates
- `pol2cart`: Polar to Cartesian coordinates

None of these functions is particularly complicated, which raises questions as to why these are not part of the existing Numpy library. Since MATLAB is a benchmark that Numpy uses for comparison, having these functions emulate the MATLAB counterparts would seem advantageous for MATLAB users looking to switch to Python+Numpy.

6.5   Python versus MATLAB Performance

- The performance of the Python script was adequate, albeit significantly slower than the MATLAB counterpart. Since the Mathworks have a significant cost associated with MATLAB, it is reasonable to expect better optimisation of the provided library functions. Even so, the Python script had adequate performance once the memory utilisation was properly optimised. Because Python is a general purpose language, the profiling and optimisation tools are freely available and easy to use.

- Because MATLAB uses a copy-on-write strategy, arrays can be "allocated" without actually consuming additional memory if the temporary array is unused. Since Numpy requires an explicit array copy to be made, it is important to deallocate arrays that are no longer needed using the `del` operator.

7 Conclusion

Within the framework of this thesis, the FEI CETA16 CMOS and the Gatan UltraScan1000 CCD camera where analysed and compared with a sub-pixel illumination method. As explained in (sec 5.4) this method delivers an accurate measurement for the characterization of the MTF curve. Results showed that a thick scintillator membrane was used for the FEI camera to account for the high conversion rate. The CR is significantly higher for lower energy that, added to a high level of background noise, impress badly on the imaging performance. This is celarly shown in the evaluated MTF that for all energy hits the 0 mark at Nyquist, far away from the 10% declared by the manufacturer A comparison with the UltraScan also reveals a wide point-spread in the scintillator. Noticeable is that a lack of manual, software-controlled possibility to activate the shutter contributes to a broader and asymmetrical PSF. For the future, more testing is perhaps a new calibration of the camera is in order, so that the performance of the SALVE project and its future achievement are not compromised. For ease of use and quickness, the two provided programs will be of good use to upcoming measurement. The time consuming and tedious task of beam tilting is now automatized and the evaluation possible in both MatLab and Python. After both versions of the code had been developed and debugged, the Python version provided adequate performance without the need for an expensive MATLAB license. The lack of several convenience MATLAB functions can be easily addressed with some simple code, and will ideally be added into future versions of the Numpy library. In the end, Python is a competitive free and open source tool for numerical computing. In conclusion we can say that useful information about the existing imaging devices has been provided. In future application a method that allows fast and easy characterization will help in the evaluation of a camera in order to achieve the best possible image representation needed for optimal TEM usage.

List of Figures

References

[1] Advantages of the cmos sensor. `https://pro.sony.com/bbsccms/assets/files/cat/camsec/solutions/E_CMOS_Sensor_WP_110427.pdf`. Accessed: 2017-01-12.

[2] Electron microscopy data files (dm3 and emi / ser). `https://ercius.wordpress.com/2012/02/17/open-electron-microscopy-data-files/`. Accessed: 2017-01-20.

[3] Milestone of microscopy's history 'salve project'. `https://translate.google.de/#de/en/Meilenstein%20der%20Mikroskopie-Geschichte%0ASALVE-Projekt`. Accessed: 2017-01-21.

[4] Optische abbildungsqualität und modulations transfer funktion (mft). `http://www.iol-test.org/imaging_quality.htm`. Accessed: 2017-01-20.

[5] Marcos A. de Araújo, Rubens Silva, Emerson de Lima, Daniel P. Pereira, and Paulo C. de Oliveira. Measurement of gaussian laser beam radius using the knife-edge technique: improvement on data analysis. *Appl. Opt.*, 48(2):393–396, Jan 2009.

[6] WJ De Ruijter and JK Weiss. Methods to measure properties of slow-scan ccd cameras for electron detection. *Review of scientific instruments*, 63(10):4314–4321, 1992.

[7] Tore Niermann, Axel Lubk, and Falk Röder. A new linear transfer theory and characterization method for image detectors. part i: Theory. *Ultramicroscopy*, 115:68–77, 2012.

[8] PTE Roberts, JN Chapman, and AM MacLeod. A ccd-based image recording system for the ctem. *Ultramicroscopy*, 8(4):385–396, 1982.

[9] Ludovica Sartini, F Simeone, P Pani, N Lo Bue, G Marinaro, A Grubich, A Lobko, G Etiope, A Capone, P Favali, et al. Nuclear instruments and methods in physics research section a: Accelerators, spectrometers, detectors and associated equipment. *Nuclear Instruments and Methods in Physics Research A*, 2010.

[10] Claude Elwood Shannon. Communication in the presence of noise. *Proceedings of the IRE*, 37(1):10–21, 1949.

[11] D.B. Williams and C.B. Carter. *Transmission Electron Microscopy: A Textbook for Materials Science. Basics.* Transmission Electron Microscopy: A Textbook for Materials Science. Springer, 1996.